Schweizerischer Erdbebendienst
Service Sismologique Suisse
Servizio Sismico Svizzero
Servizi da Terratrembels Svizzer

ETH
Eidgenössische Technische Hochschule Zürich
Swiss Federal Institute of Technology Zurich

Bern - Bundeshaus (SBERN)

SITE CHARACTERISATION REPORT

Clotaire MICHEL, Jan BURJANEK, Daniel ROTEN

Valerio POGGI, Carlo CAUZZI, Donat FÄH

Sonneggstrasse 5 CH-8092 Zürich Switzerland; E-mail: clotaire.michel@sed.ethz.ch

Last modified : November 5, 2013

Abstract

Ambient vibration array measurements were performed to characterize the sedimentary deposits at site Bern Kleine Schanze, close to the Bundeshaus. The site, where the new station SBERN of the Swiss Strong Motion Network was installed, is located at the edge of the Aare sedimentary basin. In order to characterize the velocity profile under the station, array measurements with a $200\,\mathrm{m}$ aperture were performed. The measurements were successful in deriving a velocity model for this site. The soil column underlying station SBERN is made of a first layer of moraine with low velocity around $270\,\mathrm{m/s}$ for the first 10 meters, a second layer with velocity of $400 - 500\,\mathrm{m/s}$ corresponding to fluvial sediments and finally the molasse rock at $40\,\mathrm{m}$ depth. This interface corresponds to a resonance peak at $2\,\mathrm{Hz}$. The velocity of the molasse is $800\,\mathrm{m/s}$ down to $120\,\mathrm{m}$ and increases below. A deeper resonance at $0.8\,\mathrm{Hz}$ corresponding to a deeper layer is probably present but could not be constrained with these measurements. $V_{s,30}$ is around $360\,\mathrm{m/s}$. The ground type would be C for EC8 [CEN, 2004] and SIA261 [SIA, 2003]. The theoretical SH transfer function and impedance contrast of the quarter-wavelength velocity computed from the inverted profiles show a moderate amplification especially at the resonance frequencies. Recordings on the new station will allow to validate these simple models.

Moreover, geology and H/V analysis were correlated in the whole city of Bern. The interface between the molasse rock and the quaternary sediments, very variable across the city, is responsible for the major peak in the H/V curves although the low-frequency peak at $0.8\,\mathrm{Hz}$ is also noticed throughout the city. The earthquake ground motion is therefore very variable on short distances in Bern and the station is representative only for a limited area.

Contents

1 Introduction

The station SBERN (Bern Bundeshaus) is part of the Swiss Strong Motion Network (SSMNet). SBERN was installed as a new site in the framework of the SSMNet Renewal project in 2013. This project includes also the site characterization. The passive array measurements have been selected as a standard tool to investigate these sites. Such a measurement campaign was performed on 20th February 2013 in the public park Kleine Schanze in Bern (Fig. 1), with a centre close to station SBERN, in order to characterize the sediments under this station. Moreover, a single-station measurement campaign was also performed on the whole city-centre in order to better understand the effect of the variability of the local geology on the ground motion. The city of Bern has a complex Quaternary and Tertiary geology and the station is located on the edge of the deep Aare basin. This report presents the local geology, the measurement setup, the results of the H/V analysis, including the fundamental frequencies and of the array processing of the surface waves (dispersion curves). Finally, an inversion of these results for velocity profiles is performed.

Canton	City	Location	Station code	Site type	Slope
Bern	Bern	Bundeshaus	SBERN	Edge of deep basin	Hill

Table 1: Main characteristics of the study-site.

Figure 1: Picture of the site.

2 Geology

The geology in Bern is relatively complicated (Fig. 2). The Quaternary basin of the Aare is oriented ESE/WNW, although the current flow of the river in Bern is not following this direction anymore (Fig. 3). The depth of the Quaternary, based on the gravimetric anomaly represented on this figure is not precise enough to infer the rock depth at the station considering the large shifts observed when comparing to the borehole results, but it shows that the station site is located at the edge of this basin.

Boreholes in the surroundings, available on the geoportal of Canton Bern, provide more precise values for the quaternary depth (Fig. 4). These figures show that the quaternary sediments are shallow in the surroundings of the train station, but increase quickly to the South. No borehole reaches the molasse in the ESE part of the map, indicating this part is the deep Aare basin. Close to the station SBERN, the slope of the molasse rock is estimated around $40\,^{\circ}$ using the borehole data. The closest borehole, located $170\,\mathrm{m}$ W from the SBERN station, is represented on Fig. 5. It shows soil until $4\,\mathrm{m}$, then moraine from the Würm until $12\,\mathrm{m}$, fluvial-glacial sediments down to $60\,\mathrm{m}$ and finally the molasse rock (OMM) made of sandstone.

The molasse basin is $2100\,\mathrm{m}$ deep in Bern according to Sommaruga et al. [2012], there is therefore no chance to reach the base of the Tertiary with the investigation methods used. Two layers of molasse are present on the geology map: the OMM or Upper Marine Molasse (Burdigalien or Sense-layer or Berner sandstone) and the USM or Lower Freshwater Molasse (Gümmenen layer), located below, which can be found at the surface in the new Aare riverbed in the northern part of the city. The OMM is also outcropping on the map on the NE and in the Aare river bed in the South. The geometry of the interface between these two layers is however unclear.

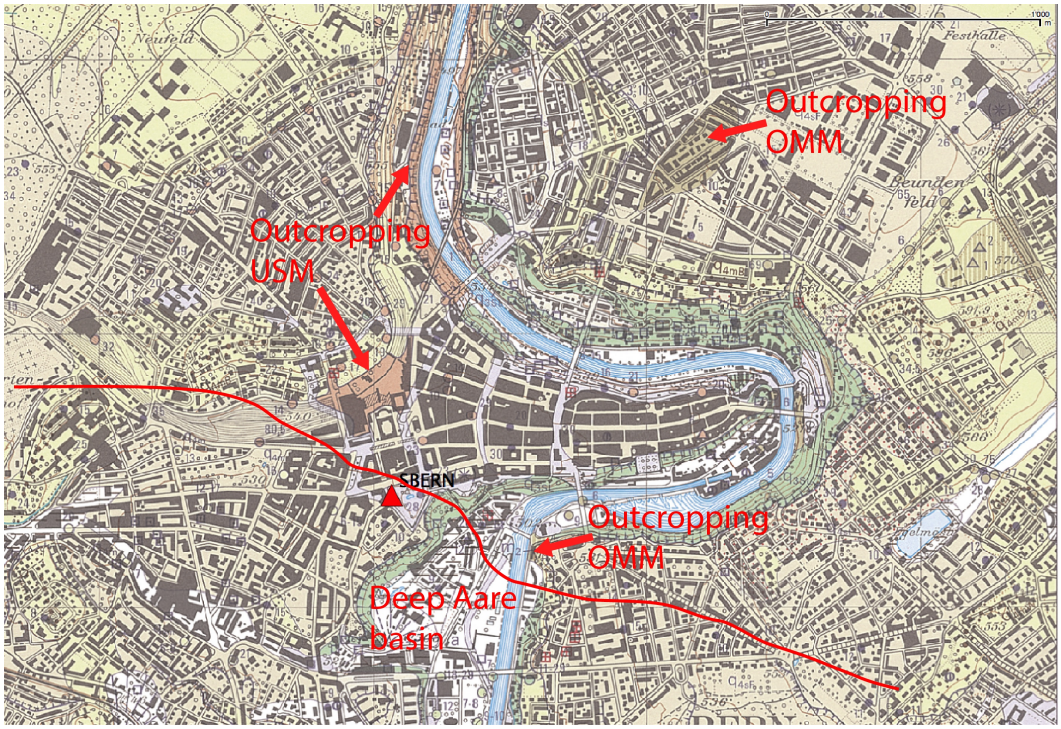

Figure 2: Geology map of the city of Bern (modified from Swisstopo). The outcropping molasse (USM: Lower Freshwater Molasse in orange; OMM: Upper Marine Molasse in brown) is stressed with additional annotations. The limit of the deep Aare basin (South) is approximately drawn in red for Quaternary depths of about $50\,\mathrm{m}$.

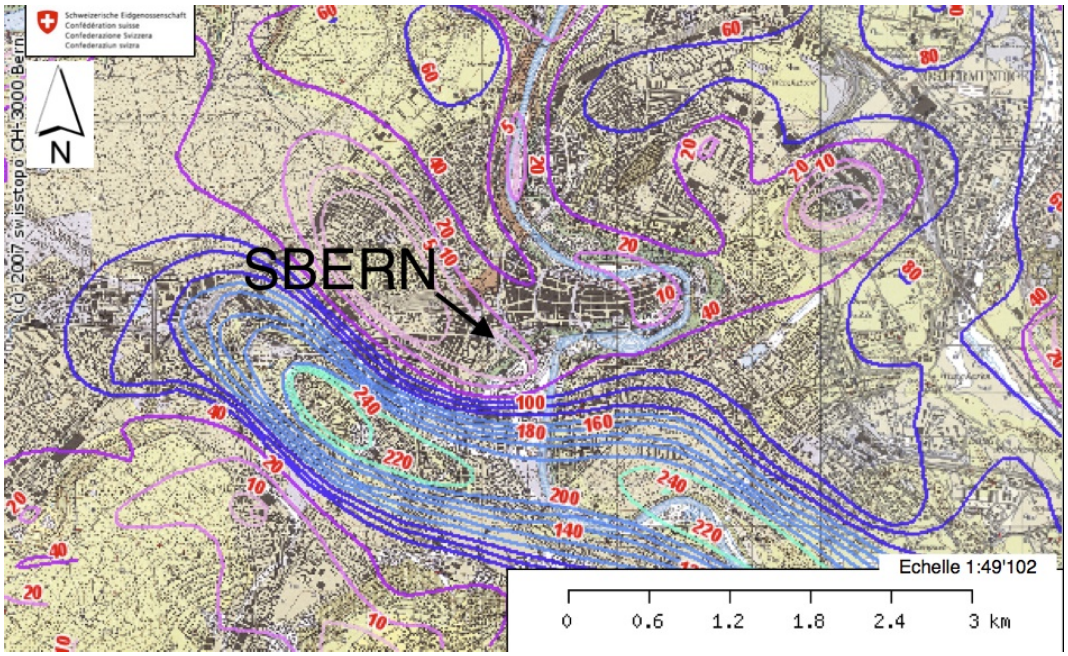

Figure 3: Depth of the Quaternary based on gravimetric anomaly. From the website geologieviewer.ch.

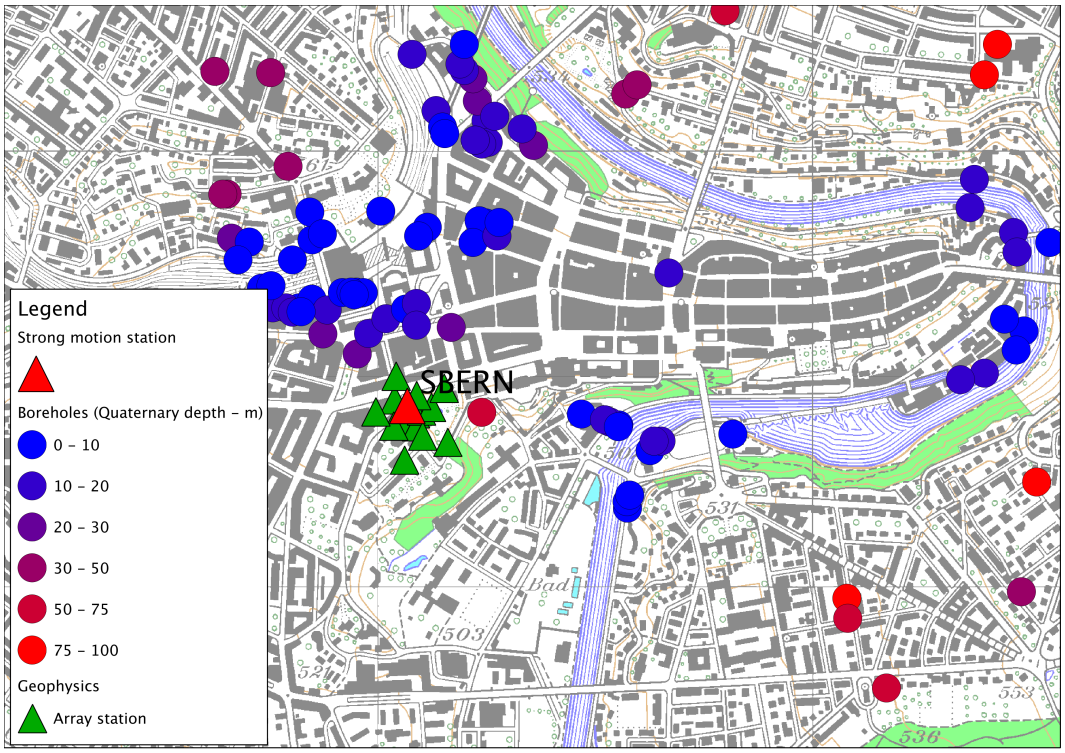

Figure 4: Depth of the Quaternary sediments based on borehole data.

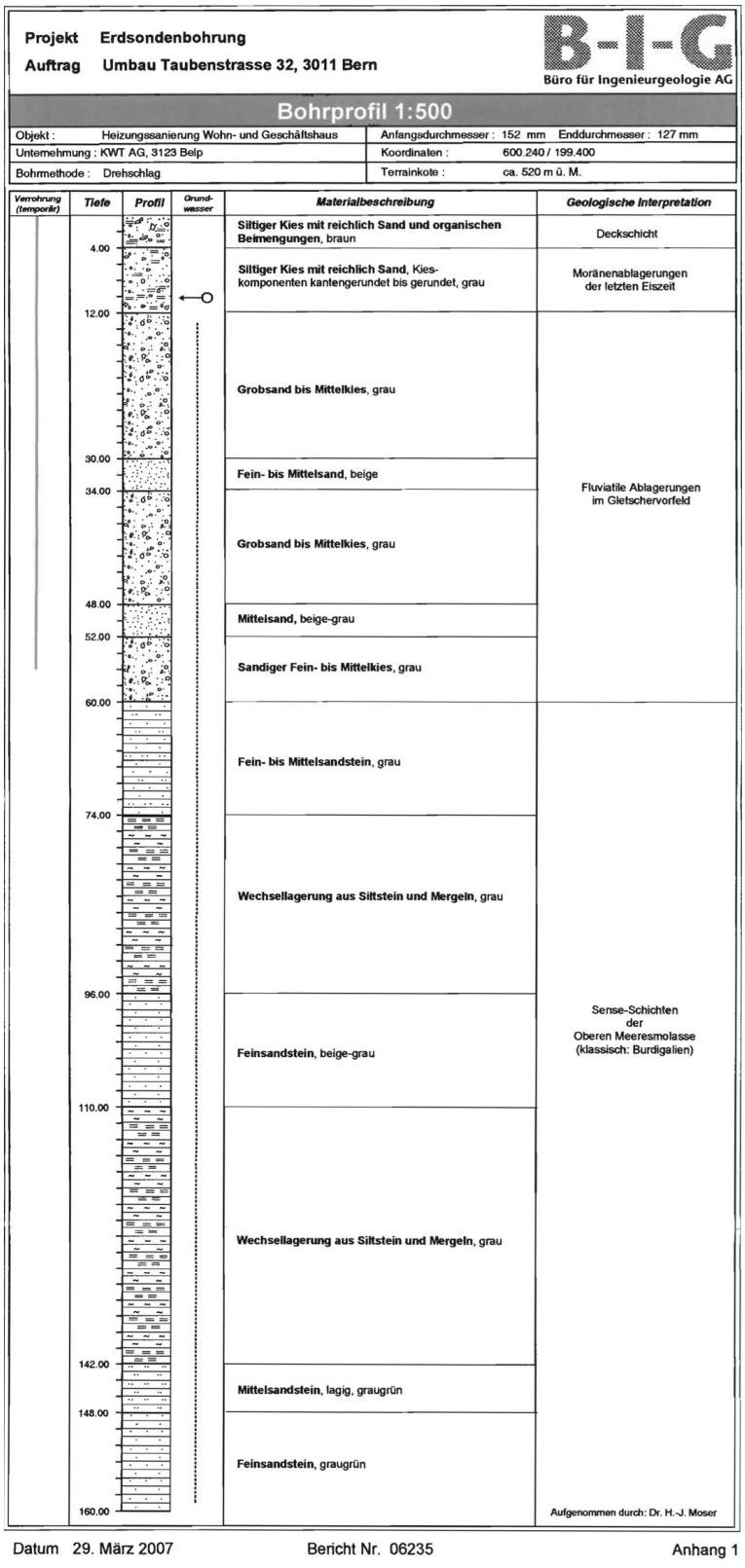

Projekt Erdsondenbohrung
Auftrag Umbau Taubenstrasse 32, 3011 Bern

B-I-G
Büro für Ingenieurgeologie AG

Bohrprofil 1:500

Objekt :	Heizungssanierung Wohn- und Geschäftshaus	Anfangsdurchmesser : 152 mm	Enddurchmesser : 127 mm
Unternehmung :	KWT AG, 3123 Belp	Koordinaten :	600.240 / 199.400
Bohrmethode :	Drehschlag	Terrainkote :	ca. 520 m ü. M.

Verrohrung (temporär)	Tiefe	Profil	Grundwasser	Materialbeschreibung	Geologische Interpretation
	4.00			**Siltiger Kies mit reichlich Sand und organischen Beimengungen**, braun	Deckschicht
	12.00			**Siltiger Kies mit reichlich Sand**, Kieskomponenten kantengerundet bis gerundet, grau	Moränenablagerungen der letzten Eiszeit
	30.00			**Grobsand bis Mittelkies**, grau	Fluviatile Ablagerungen im Gletschervorfeld
	34.00			**Fein- bis Mittelsand**, beige	
	48.00			**Grobsand bis Mittelkies**, grau	
	52.00			**Mittelsand**, beige-grau	
	60.00			**Sandiger Fein- bis Mittelkies**, grau	
	74.00			**Fein- bis Mittelsandstein**, grau	Sense-Schichten der Oberen Meeresmolasse (klassisch: Burdigalien)
	96.00			**Wechsellagerung aus Siltstein und Mergeln**, grau	
	110.00			**Feinsandstein**, beige-grau	
	142.00			**Wechsellagerung aus Siltstein und Mergeln**, grau	
	148.00			**Mittelsandstein**, lagig, graugrün	
	160.00			**Feinsandstein**, graugrün	Aufgenommen durch: Dr. H.-J. Moser

Datum 29. März 2007 Bericht Nr. 06235 Anhang 1

Figure 5: Borehole profile close to station SBERN.

3 Experiment description

3.1 Ambient Vibrations

The ground surface is permanently subjected to ambient vibrations due to:

- natural sources (ocean and large-scale atmospheric phenomena) below $1\,\mathrm{Hz}$,
- local meteorological conditions (wind and rain) at frequencies around $1\,\mathrm{Hz}$,
- human activities (industrial machines, traffic…) at frequencies above $1\,\mathrm{Hz}$ [Bonnefoy-Claudet et al., 2006].

The objective of the measurements is to record these ambient vibrations and to use their propagation properties to infer the underground structure. First, the polarization of the recorded waves (H/V ratio) are used to derive the resonance frequencies of the ground layers. Second, the arrival time delays between stations is used to derive the velocity of surface waves at different frequencies (dispersion). The information (H/V, dispersion curves) is then used to derive the properties of the soil layers using an inversion process.

3.2 Equipment

For these measurements 12 Quanterra Q330 dataloggers named NR01 to NR12 and 14 Lennartz 3C 5 s seismometers were available (see Tab. 2). Each datalogger can record on 2 ports A (channels EH1, EH2, EH3 for Z, N, E directions) and B (channels EH4, EH5, EH6 for Z, N, E directions). The time synchronization was ensured by GPS. The sensors are placed on a metal tripod for a better coupling with the ground. For the H/V survey, a Quanterra Q330 datalogger was used with a Lennartz 3C 5 s seismometer. No tripods were used, since the sensors were placed mainly on the asphalt.

Survey	**Digitizer**	**Model**	**Number**	**Resolution**
Array		Quanterra Q330	12	$24\,\mathrm{bits}$
Single station		Quanterra Q330	1	$24\,\mathrm{bits}$
Survey	**Sensor type**	**Model**	**Number**	**Cut-off frequency**
Array	Velocimeter	Lennartz 3C	14	$0.2\,\mathrm{Hz}$
Single station	Velocimeter	Lennartz 3C	1	$0.2\,\mathrm{Hz}$

Table 2: Equipment used.

3.3 Geometry of the recordings

Two array configurations were used, for a total of 4 rings of 10, 25, 50 and $100\,\mathrm{m}$ radius around a central station. The first configuration includes the 3 inner rings with 14 sensors; the second configuration includes the 2 outer rings (plus the central station and the inner ring) with 14 sensors. The minimum inter-station distance and the aperture are therefore 10 and $100\,\mathrm{m}$ and

10 and 200 m, respectively. The experimental setup is displayed in Fig. 6. The final usable datasets are detailed in section 4.2.
The single station campaign aimed at measuring on a grid in the city centre (Fig. 7).

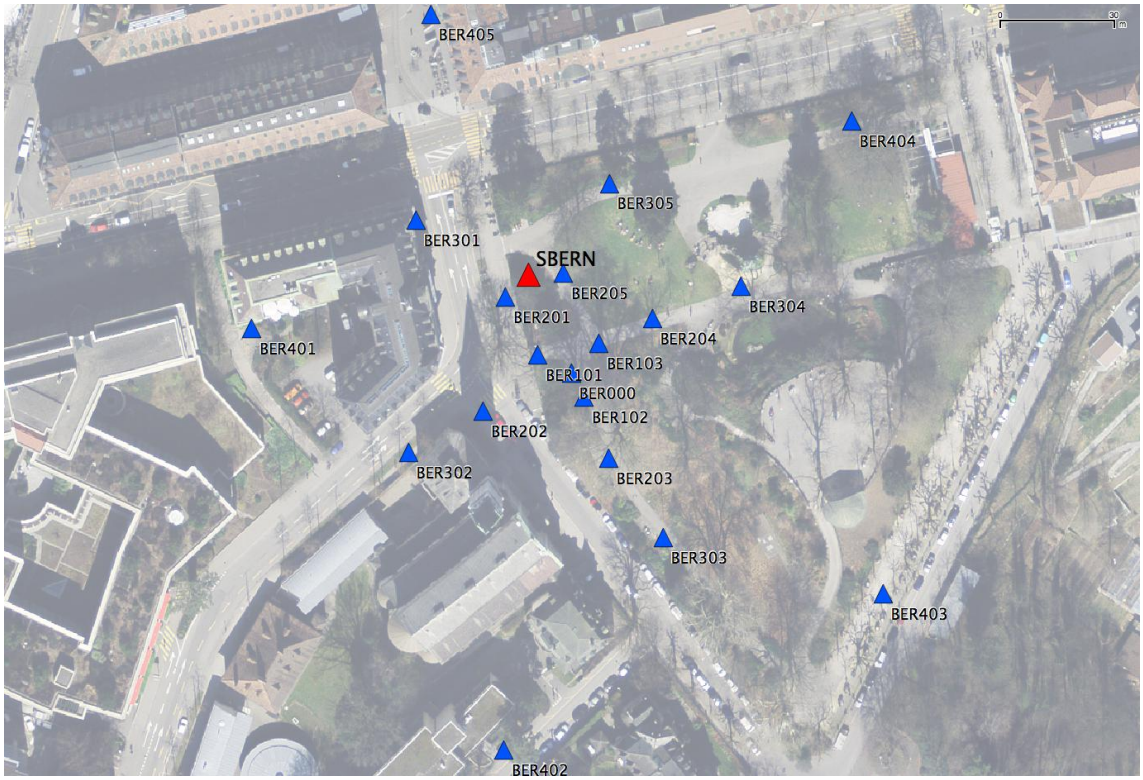

Figure 6: Geometry of the arrays.

3.4 Positioning of the stations

The sensor coordinates were measured using a differential GPS device (Leica Viva), including only a rover station and using the Real Time Kinematic technique provided by Swisstopo. It allows an absolute positioning with an accuracy of about 3 cm on the Swissgrid. However, the system did not work for some points too close to buildings or below trees. Around 10 minutes GPS recordings were performed and post-processed using a virtual reference provided by Swisstopo (RINEX data) and the LGO software. The positioning is greatly improved, except for points BER402 to 405 for which the raw data logging was not active (accuracy of 1.7 m at point BER404, the others being reasonably accurate). Moreover, point BER401 was placed by hand on the swissimage from the pictures.
For the single station campaign, the positioning was done by picking location on the 1:25000 map, with an accuracy of 5 m.

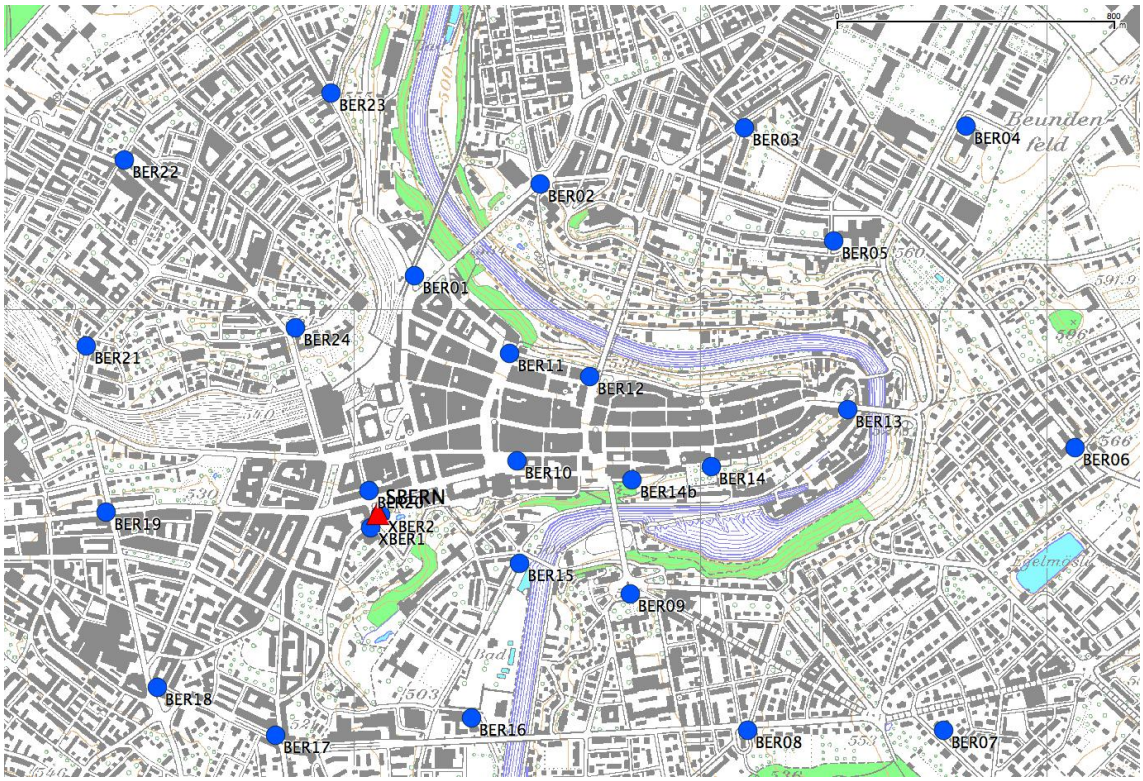

Figure 7: Position of the single station measurements.

4 Data quality

4.1 Usable data

The largest time windows were extracted, for which all the sensors of the array were in position and the GPS synchronization was ensured. GPS measurement were performed during the datasets due to their duration.

Points BER201, 202 and 301 were close to a major road, with cars going at high speed (about $50\,\mathrm{km/h}$) and are therefore more noisy at low frequencies due to the air flow and at high frequencies due to ground vibrations. Spurious peaks due to machines can be seen in all directions especially at 1.92, 2.78, 3.21 and $9.4\,\mathrm{Hz}$.

For the H/V campaign, traffic and pedestrians lowered the quality of the data. The GPS was not synchronized for these measurements. A machine at $1.2\,\mathrm{Hz}$ is disturbing the H/V computation in BER07, BER14 and BER14b.

The characteristics of the datasets are detailed in Tab. 3.

4.2 Data processing

The data were first converted to SAC format including in the header the coordinates of the point (CH1903 system), the recording component and a name related to the position. The name is made of 3 letters characterizing the location (BER here), 1 digit for the ring and 2 more digits for the number in the ring. For the single station measurement, the same letters were chosen and the numbers are increasing from 01 to 24. The recordings were not corrected from the response of the acquisition chain and the values (in counts) were not converted to $\mathrm{m/s}$.

Dataset	**Starting Date**	**Time**	**Length**	F_s	**Min. inter-distance**	**Aperture**	**# of points**
1	2013/02/20	9:03	113 min	200 Hz	10 m	100 m	14
2	2013/02/20	14:34	119 min	200 Hz	10 m	200 m	14
BER01	2011/05/24	08:54	33 min	200 Hz			1
BER02	2011/05/24	09:42	31 min	200 Hz			1
BER03	2011/05/24	10:32	32 min	200 Hz			1
BER04	2011/05/24	12:14	31 min	200 Hz			1
BER05	2011/05/24	11:16	32 min	200 Hz			1
BER06	2011/05/24	13:05	31 min	200 Hz			1
BER07	2011/05/24	13:47	20 min	200 Hz			1
BER08	2011/05/24	14:26	32 min	200 Hz			1
BER09	2011/05/24	15:12	31 min	200 Hz			1
BER10	2011/05/24	15:59	32 min	200 Hz			1
BER11	2011/05/25	06:56	36 min	200 Hz			1
BER12	2011/05/25	07:45	32 min	200 Hz			1
BER13	2011/05/25	10:13	32 min	200 Hz			1
BER14	2011/05/25	08:39	34 min	200 Hz			1
BER14b	2011/05/25	09:28	29 min	200 Hz			1
BER15	2011/05/25	11:14	37 min	200 Hz			1
BER16	2011/05/25	12:07	32 min	200 Hz			1
BER17	2011/05/25	13:09	30 min	200 Hz			1
BER18	2011/05/25	13:59	31 min	200 Hz			1
BER19	2011/05/25	14:45	30 min	200 Hz			1
BER20	2011/05/25	15:32	28 min	200 Hz			1
BER21	2011/05/26	07:22	30 min	200 Hz			1
BER22	2011/05/26	08:12	32 min	200 Hz			1
BER23	2011/05/26	08:59	31 min	200 Hz			1
BER24	2011/05/26	09:48	25 min	200 Hz			1

Table 3: Usable datasets.

5 H/V processing

5.1 Processing method and parameters

In order to process the H/V spectral ratios, several codes and methods were used. The classical H/V method was applied using the Geopsy `http://www.geopsy.org` software. In this method, the ratio of the smoothed Fourier Transform of selected time windows are averaged. Tukey windows (cosine taper of 5% width) of $50\,\mathrm{s}$ long overlapping by 50% were selected. Konno and Ohmachi [1998] smoothing procedure was used with a b value of 60. The classical method computed using the method of Fäh et al. [2001] was also performed.

Moreover, the time-frequency analysis method [Fäh et al., 2009] was used to estimate the ellipticity function more accurately using the Matlab code of V. Poggi. In this method, the time-frequency analysis using the Wavelet transform is computed for each component. For each frequency, the maxima over time (10 per minute with at least $0.1\,\mathrm{s}$ between each) in the TFA are determined. The Horizontal to Vertical ratio of amplitudes for each maximum is then computed and statistical properties for each frequency are derived. A Cosine wavelet with parameter 9 is used [Poggi et al., 2012b]. The mean of the distribution for each frequency is stored. For the sake of comparison, the time-frequency analysis of Fäh et al. [2001], based on the spectrogram, was also used, as well as the wavelet-based TFA coded in Geopsy.

The ellipticity extraction using the Capon analysis [Poggi and Fäh, 2010] (see section on array analysis) was also performed.

Method	Freq. band	Win. length	Anti-trig.	Overlap	Smoothing
Standard H/V Geopsy	$0.2 - 20\,\mathrm{Hz}$	$50\,\mathrm{s}$	No	50%	K&O 60
Standard H/V D. Fäh	$0.2 - 20\,\mathrm{Hz}$	$30\,\mathrm{s}$	No	75%	-
H/V TFA Geopsy	$0.2 - 20\,\mathrm{Hz}$	Morlet m=8 fi=1	No	-	-
H/V TFA D. Fäh	$0.2 - 20\,\mathrm{Hz}$	Specgram	No	-	-
H/V TFA V. Poggi	$0.2 - 20\,\mathrm{Hz}$	Cosine wpar=9	No	-	No

Table 4: Methods and parameters used for the H/V processing.

5.2 H/V results in the city

As explained in section 2, the depth of the quaternary sediments is very variable across the city leading to very variable H/V ratios. From the analysis of these H/V ratios, conclusions can however be drawn. First of all, a first peak frequency around $0.8\,\mathrm{Hz}$ for the whole zone has been found, corresponding to a nearly flat and deep interface (Fig. 8). Point BER11 does not show any peak, it is likely on an underground civil structure. It is not clear wether the variations of this frequency value (lower values in the Western part) are related to picking errors, difference in the depth of the interface or variability in the velocity profile of the above layers. This low frequency peak is related to an interface within the Tertiary rock (molasse). I can be roughly estimated at 200 to $400\,\mathrm{m}$ depth.

Moreover, in most cases, a clear second peak could be picked and displayed on a map (Fig. 9). This second peak seems to be correlated with the depth of the molasse. In the WSW

part, the resonance frequency of the deep Aare quaternary basin is mixed with the frequency corresponding to the deep interface at $0.8\,\mathrm{Hz}$ (BER16, BER19). The peak of the quaternary sediments is even at lower frequencies in BER18 ($0.7\,\mathrm{Hz}$) and BER17 ($0.5\,\mathrm{Hz}$). The amplitudes are the largest for these points. A borehole indicates the molasse at $250\,\mathrm{m}$ in this region. The basin is still relatively deep in BER21 ($1.2\,\mathrm{Hz}$).

In the other parts of the city, the molasse depth is not as simple to describe. Some points are located close to molasse outcrops and show therefore high frequency values such as in BER03 ($12\,\mathrm{Hz}$), BER23 ($6\,\mathrm{Hz}$).

The H/V ratios are therefore interpreted relatively to two interfaces, a deep interface, relatively flat in the Tertiary rock at 200 to $400\,\mathrm{m}$ depth and the interface between the Quaternary sediments and the Tertiary rock, from 0 to $300\,\mathrm{m}$ depth in this region. These interfaces are crossing in the South, in the deep Aare basin.

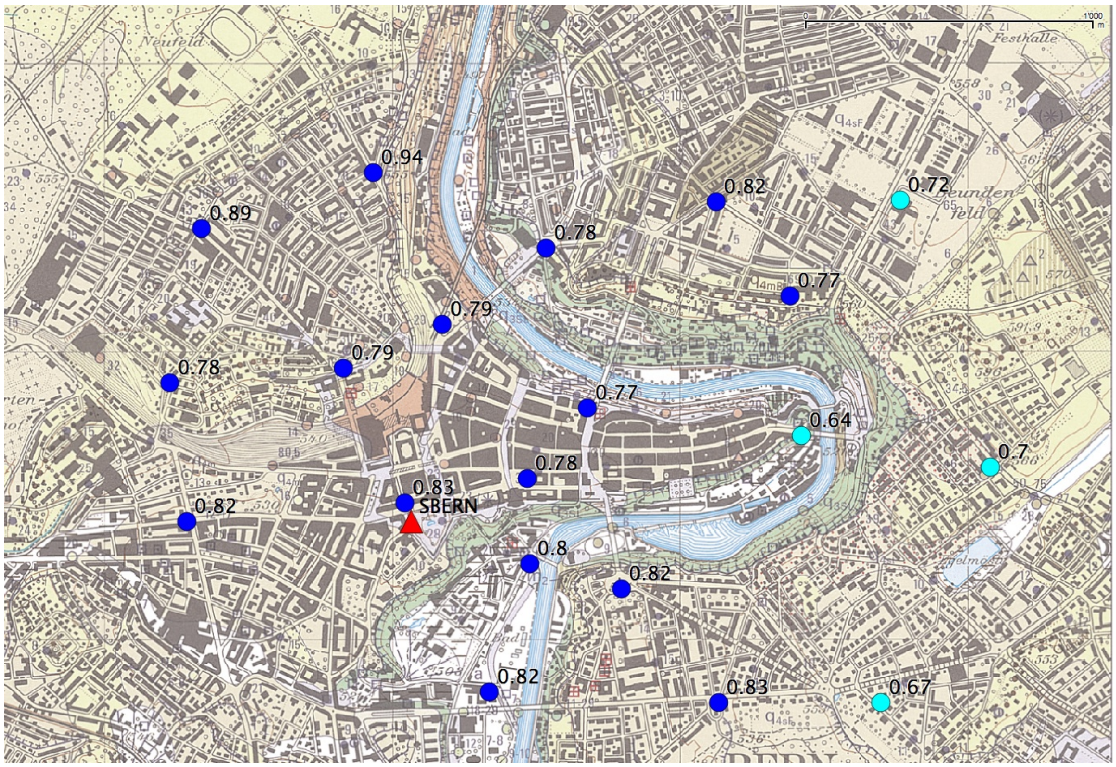

Figure 8: Map of the H/V peak related to the deep interface with geology in background.

5.3 H/V results in the array

From the spectra of the array recordings, a clear increase in amplitude appears around $2\,\mathrm{Hz}$ indicating that the major velocity contrast corresponds to this frequency peak. At $0.84\,\mathrm{Hz}$, a small peak appears for the less noisy stations, corresponding to the peak found previously. However, the energy at this frequency is low.

H/V curves are varying across the array (Fig. 10), showing that the lateral variability is important. The H/V peaks are broad and therefore not very clear. The fundamental frequency

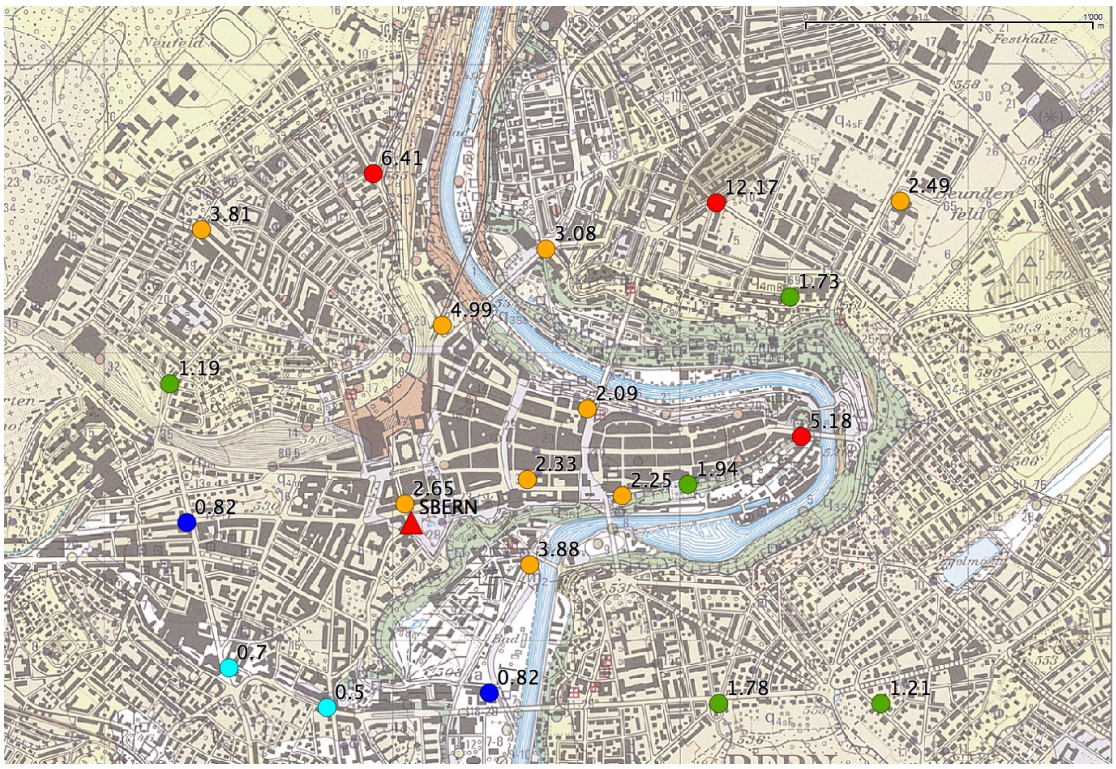

Figure 9: Map of the H/V peak related to the quaternary sediment cover with geology in background.

remains the same as previously picked at $0.8 - 0.9\,\mathrm{Hz}$ with amplitudes around 3, even though it could not be found at some points like BER401. The second peak is also not very clear and disturbed by a machine at $2.7\,\mathrm{Hz}$. No clear zonation can be seen from these measurements.

Moreover, all the methods to compute H/V ratios are compared on Fig. 11, in which the classical methods were divided by $\sqrt{2}$ to account for Love wave contribution. The matching is reasonable except the parametrization of the codes of D. Fäh were kept with default values and not adapted to the low frequencies.

5.4 Polarization analysis

Considering the shape of the Aare basin, a 2D resonance could occur, although the array is located at the edge of the basin, where these effects are limited. Therefore, polarization analysis on the array data was performed using the method of Burjánek et al. [2010]. All points (Fig. 12) show very weak polarization that cannot be linked to the Aare basin. The two orthogonal motions appearing clearly on the strike of the polarization (Fig. 12) are likely due to the machines previously observed at $1.92\,\mathrm{Hz}$. It is therefore excluded that the observed resonance frequencies are related to 2D resonance. The points from the single station measurements were processed as well but do not show any evidence of 2D resonance in the Aare basin.

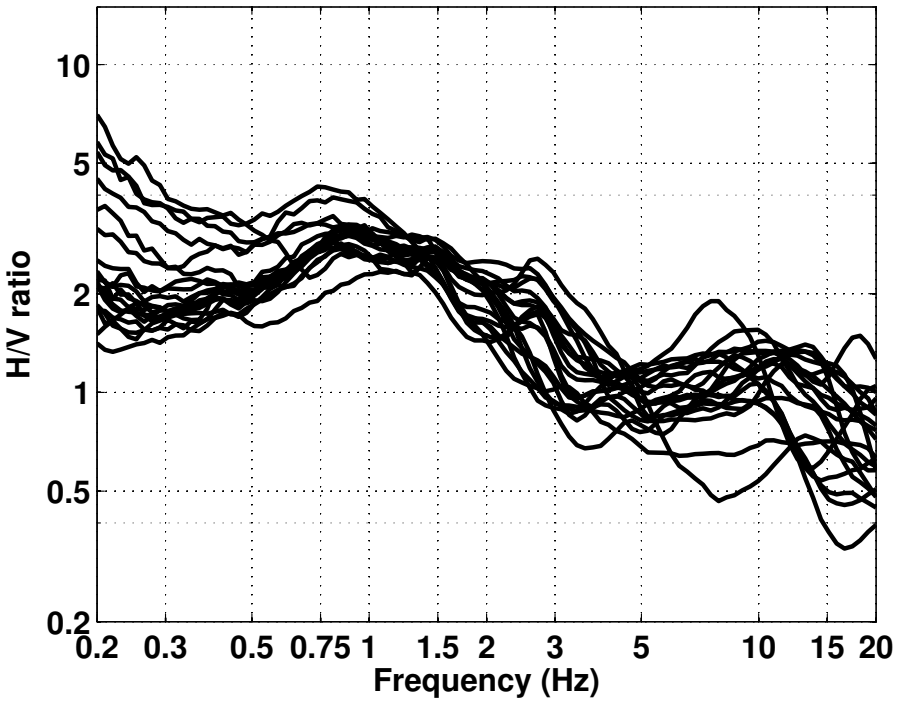

Figure 10: H/V spectral ratios (time-frequency analysis code V. Poggi).

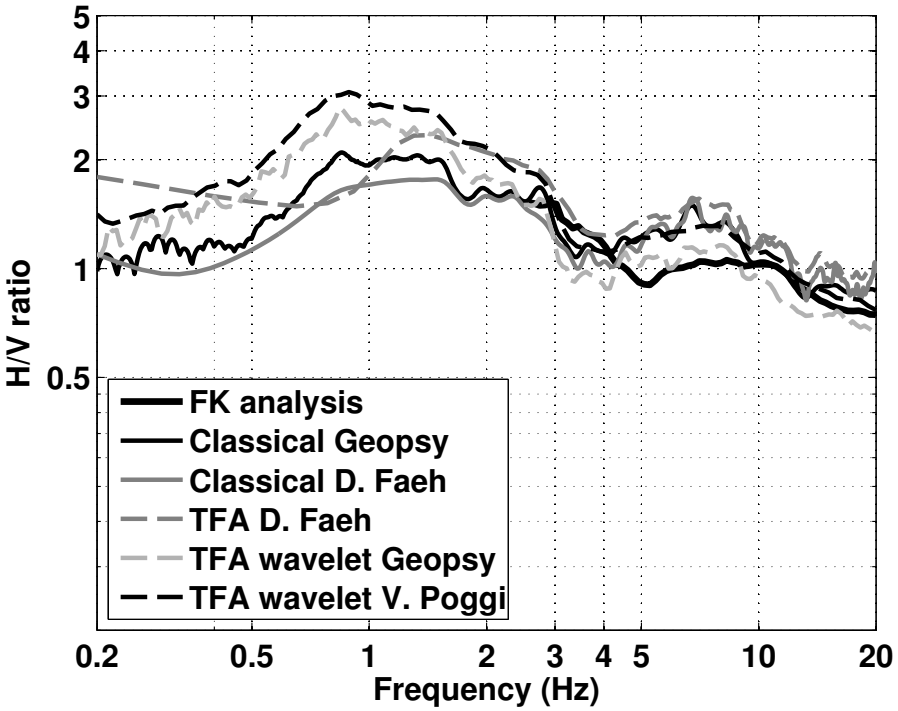

Figure 11: H/V spectral ratios for point BER000 using the different codes. Classical methods were divided by $\sqrt{2}$.

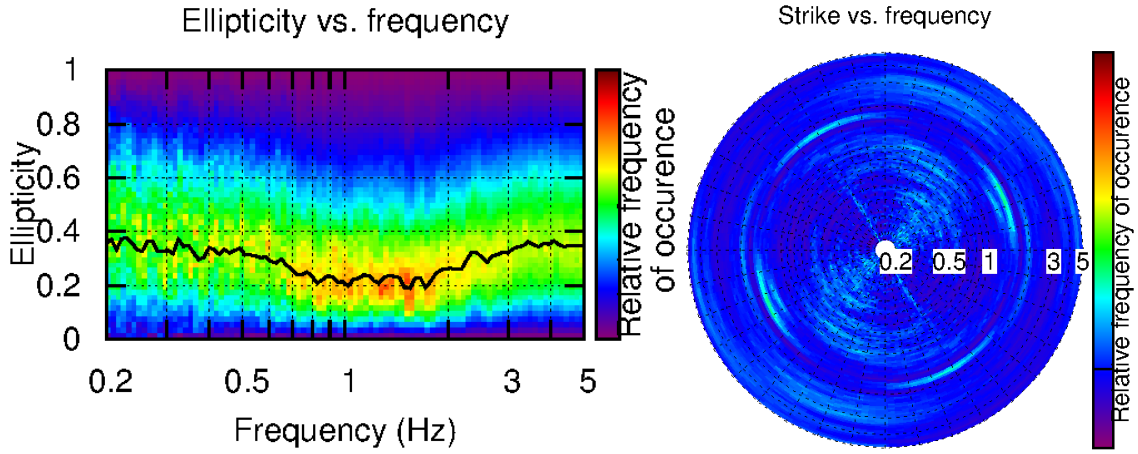

Figure 12: Polarization analysis at point BER000. Left: Ellipticity (A trough in the ellipticity corresponds to polarized motion). Right: Strike of the polarization.

6 Array processing

6.1 Processing methods and parameters

The vertical components of the arrays were processed using the FK and the High-resolution FK analysis [Capon, 1969] using the Geopsy `http://www.geopsy.org` software. Better results were obtained using large time windows (300T). The results of computations of both datasets were merged to estimate the dispersion curves.

Moreover, a 3C array analysis [Fäh et al., 2008] was also performed using the array_tool_3C software [Poggi and Fäh, 2010]. It allows to derive Rayleigh and Love modes including the Rayleigh ellipticity. The results of computations of both datasets were merged to estimate the dispersion curves.

Method	Set	Freq. band	Win. length	Anti-trig.	Overlap	Grid step	Grid size	# max.
HRFK 1C	1	$1-25\,\mathrm{Hz}$	$300T$	No	50%	0.001	0.6	5
HRFK 1C	2	$1-25\,\mathrm{Hz}$	$300T$	No	50%	0.001	0.6	5
HRFK 3C	1	$1-25\,\mathrm{Hz}$	Wav. 10	No	50%	200	2000	5
			Tap. 0.2			m/s	m/s	
HRFK 3C	2	$1-25\,\mathrm{Hz}$	Wav. 10	No	50%	200	2000	5
			Tap. 0.2			m/s	m/s	

Table 5: Methods and parameters used for the array processing.

6.2 Obtained dispersion curves

The first mode (Rayleigh) in the 1C FK analysis could be picked with its standard deviation between 2.5 and $9\,\mathrm{Hz}$ and further until $14.5\,\mathrm{Hz}$ but without standard deviation and with less confidence (Fig. 13). The phase velocities are ranging from $1100\,\mathrm{m/s}$ at $2.5\,\mathrm{Hz}$ down to $280\,\mathrm{m/s}$ at $14.5\,\mathrm{Hz}$.

Using the 3C analysis, both fundamental Rayleigh and Love modes can be picked (Fig. 13). For Rayleigh mode, the velocities are found 15% higher than those found with the 1C analysis below $4\,\mathrm{Hz}$ (Fig. 14). Love mode can be picked between 2.1 and $10\,\mathrm{Hz}$ (Fig. 14).

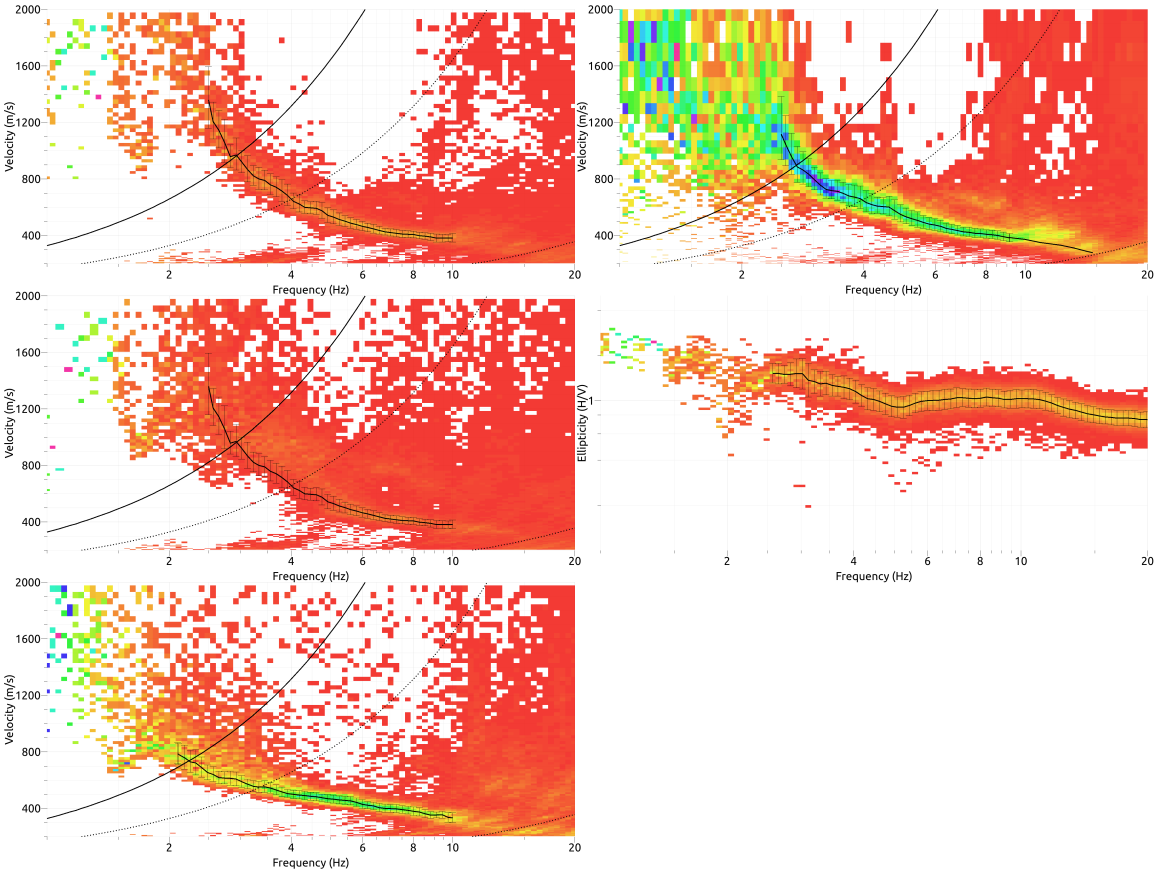

Figure 13: Dispersion curves obtained from the 3C array analysis (on the left from top to bottom: vertical, radial, transverse) and 1C array analysis (top right). Ellipticity obtained from the 3C array analysis (centre-right).

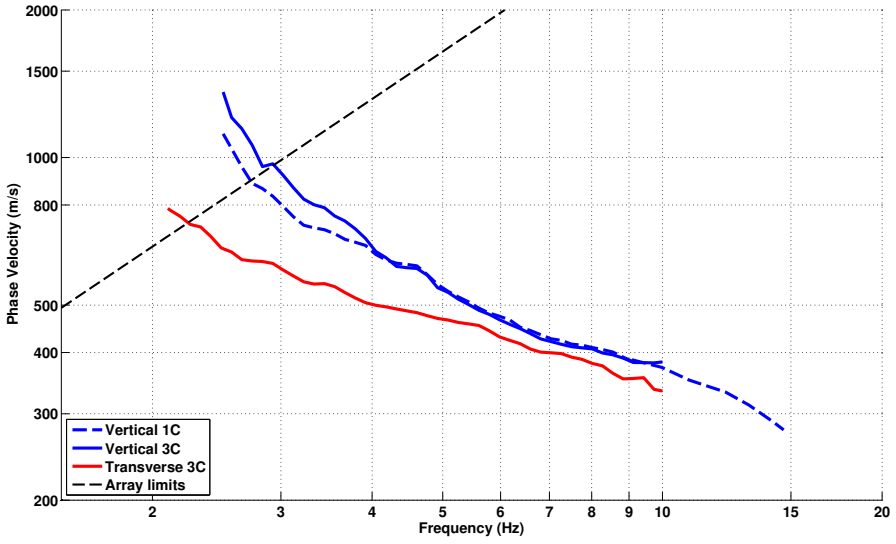

Figure 14: Picked Rayleigh and Love dispersion curves from 1C and 3C methods.

7 Inversion and interpretation

7.1 Inversion

For the inversion, Rayleigh and Love fundamental modes dispersion curves and the right flank of the ellipticity (Poggi TFA method in BER000) were used as simultaneous targets without standard deviation to avoid different weighting. The Rayleigh mode from the 1C analysis was used since it looked clearer in the FK analysis (Fig. 13). All curves were resampled using 50 points between 0.5 and $15\,\mathrm{Hz}$ in log scale.

The inversion was performed using the Improved Neighborhood Algorithm (NA) [Wathelet, 2008] implemented in the Dinver software. In this algorithm, the tuning parameters are the following: Ns_0 is the number of starting models, randomly distributed in the parameter space, Nr is the the number of best cells considered around these Ns_0 models, Ns is the number of new cells generated in the neighborhood of the Nr cells (Ns/Nr per cell) and It_{max} is the number of iteration of this process. The process ends with $Ns_0 + Nr * \frac{Ns}{Nr} * It_{max}$ models. The used parameters are detailed in Tab. 6.

It_{max}	Ns_0	Ns	Nr
500	10000	100	100

Table 6: Tuning parameters of Neighborhood Algorithm.

During the inversion process, low velocity zones were not allowed. The Poisson ratio was inverted in each layer in the range 0.2-0.4. The density was supposed equal to $2000\,\mathrm{kg/m^3}$ except for the deepest layers ($2500\,\mathrm{kg/m^3}$). Inversions with free layer depths as well as fixed layer depths were performed. 4 layers are enough to explain the targets (dispersion curves), but more layers are used to smooth the obtained results and better explore the parameter space. 5 independent runs of 5 different parametrization schemes (4 and 5 layers over a half space and 10, 11 and 12 layers with fixed depth) were performed. For further elaborations, the best models of these 25 runs were selected (Fig. 18).

When comparing to the target curves (Fig. 16 and Fig. 17), all curves are well represented. The ellipticity has however to be discussed. We first tried to reproduce the first observed peak in the H/V analysis at $0.8\,\mathrm{Hz}$ and its right flank. However, it is poorly constrained. A single interface may explain the ellipticity but the Rayleigh dispersion curve would not be compatible with the observations. Tests however show that such an interface would appear at a depth of about $350 - 400\,\mathrm{m}$. A gradient increase in the velocity may give the correct Rayleigh dispersion and ellipticity, but there were too many unknowns, it was therefore decided to stop at $160\,\mathrm{m}$ depth.
Moreover, the inversion confirms the second peak found in the H/V analysis. It is found even without using the ellipticity information but the right flank allows to constrain it better. In order to fit the right flank, its peak frequency is actually found around $2\,\mathrm{Hz}$, instead of $2.7\,\mathrm{Hz}$ as initially picked in the H/V. This discrepancy is not surprising since the picking in the H/V was very uncertain.

The retrieved velocity profiles reach a depth of $160\,\mathrm{m}$, in the molasse rock with velocities of about $1000 - 1500\,\mathrm{m/s}$. They are correlated in the following with the borehole presented

on Fig. 5. At lower depths, above $120\,\mathrm{m}$, a thick molasse layer at about $800\,\mathrm{m/s}$ is found. The interface with the sediments is found around $40\,\mathrm{m}$ with velocity of the sediments around $400 - 500\,\mathrm{m/s}$, corresponding to fluvial sediments (gravels) in the borehole. Another clear interface is found at $10\,\mathrm{m}$ where the velocity decreases down to $270\,\mathrm{m/s}$. It corresponds to moraine of the latest glaciation.

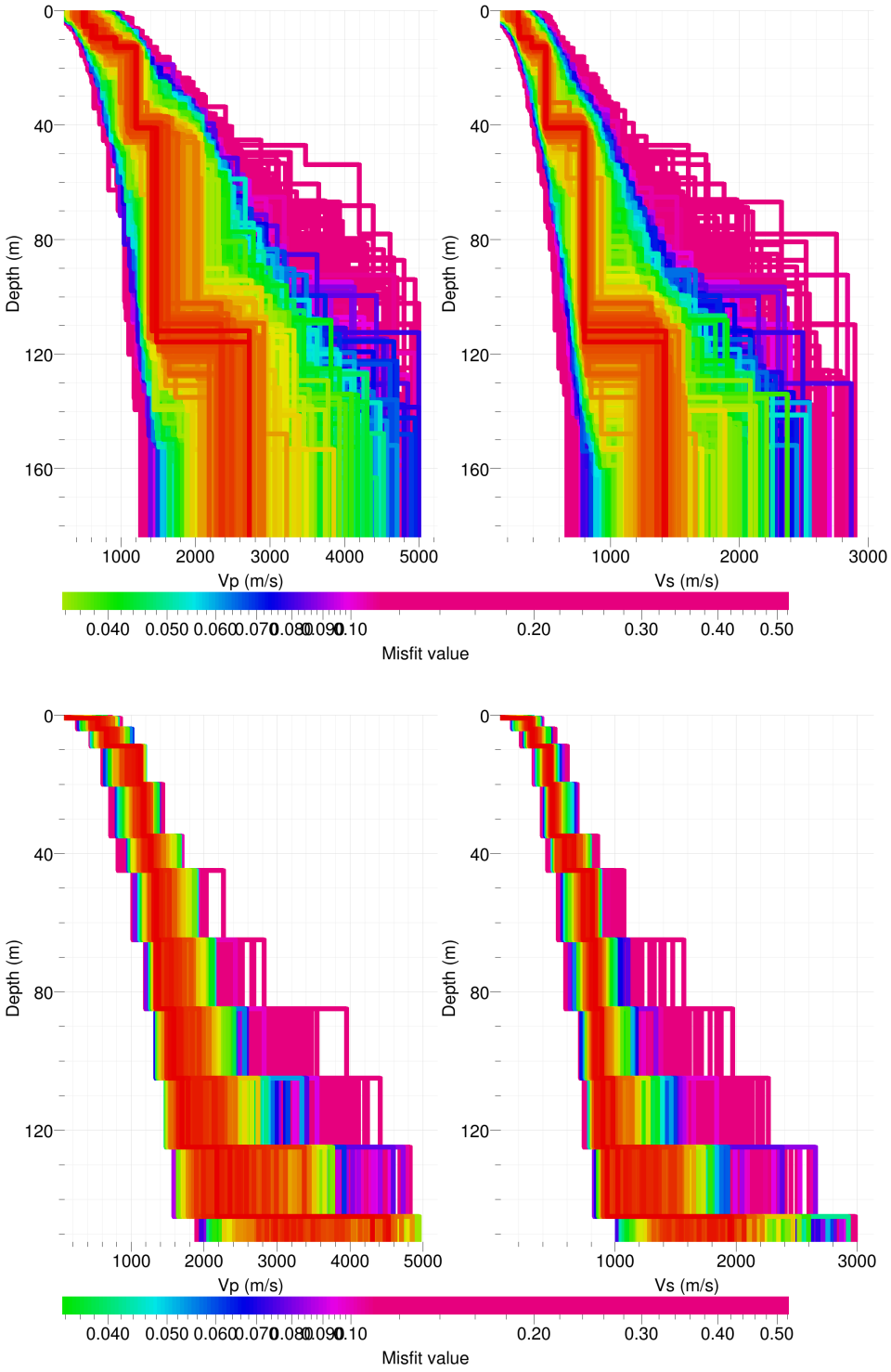

Figure 15: Inverted ground profiles in terms of V_p and V_s; top: free layer depth strategy; bottom: fixed layer depth strategy.

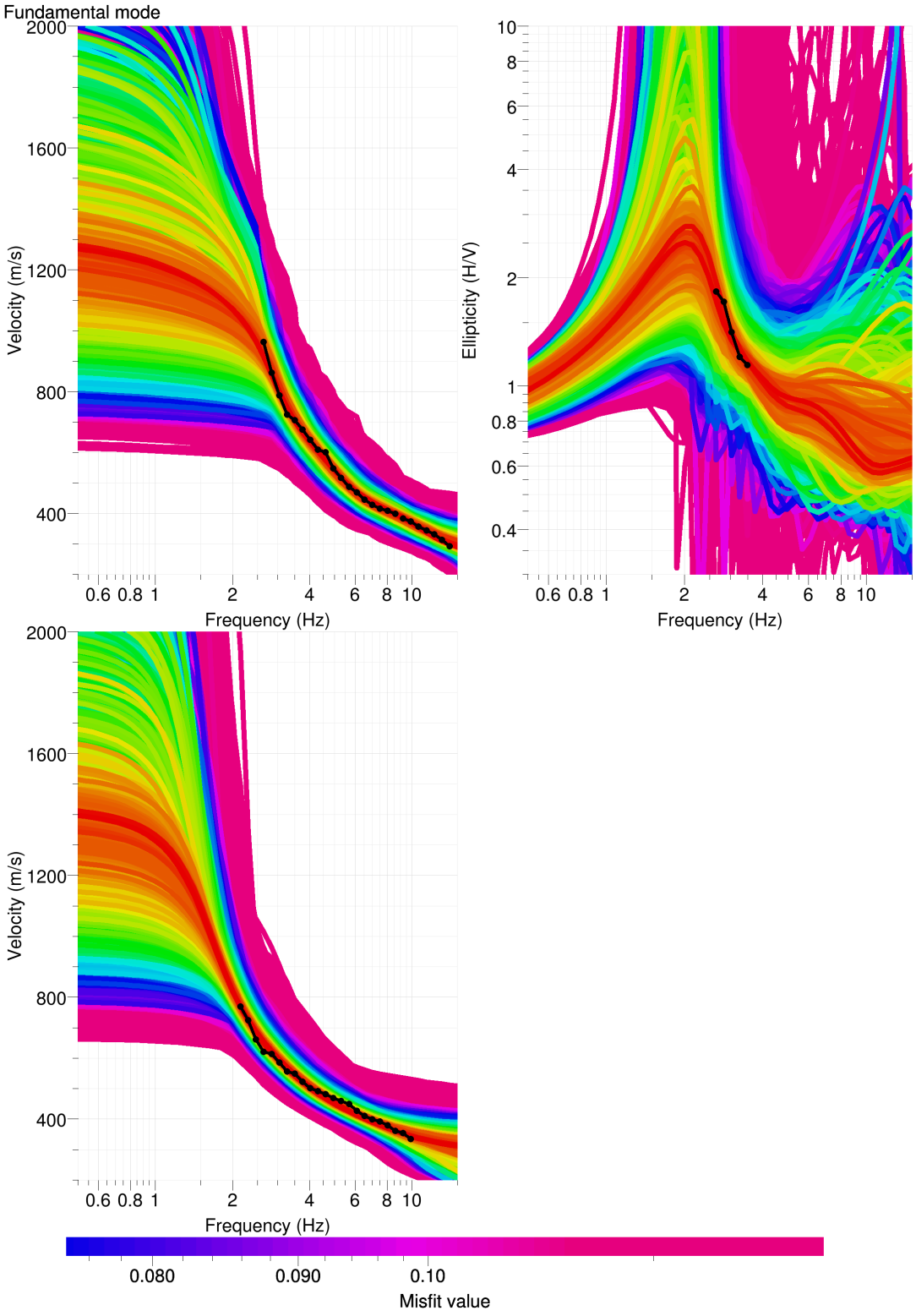

Figure 16: Comparison between inverted models and measured Rayleigh and Love modes and corresponding ellipticity, free layer depth strategy.

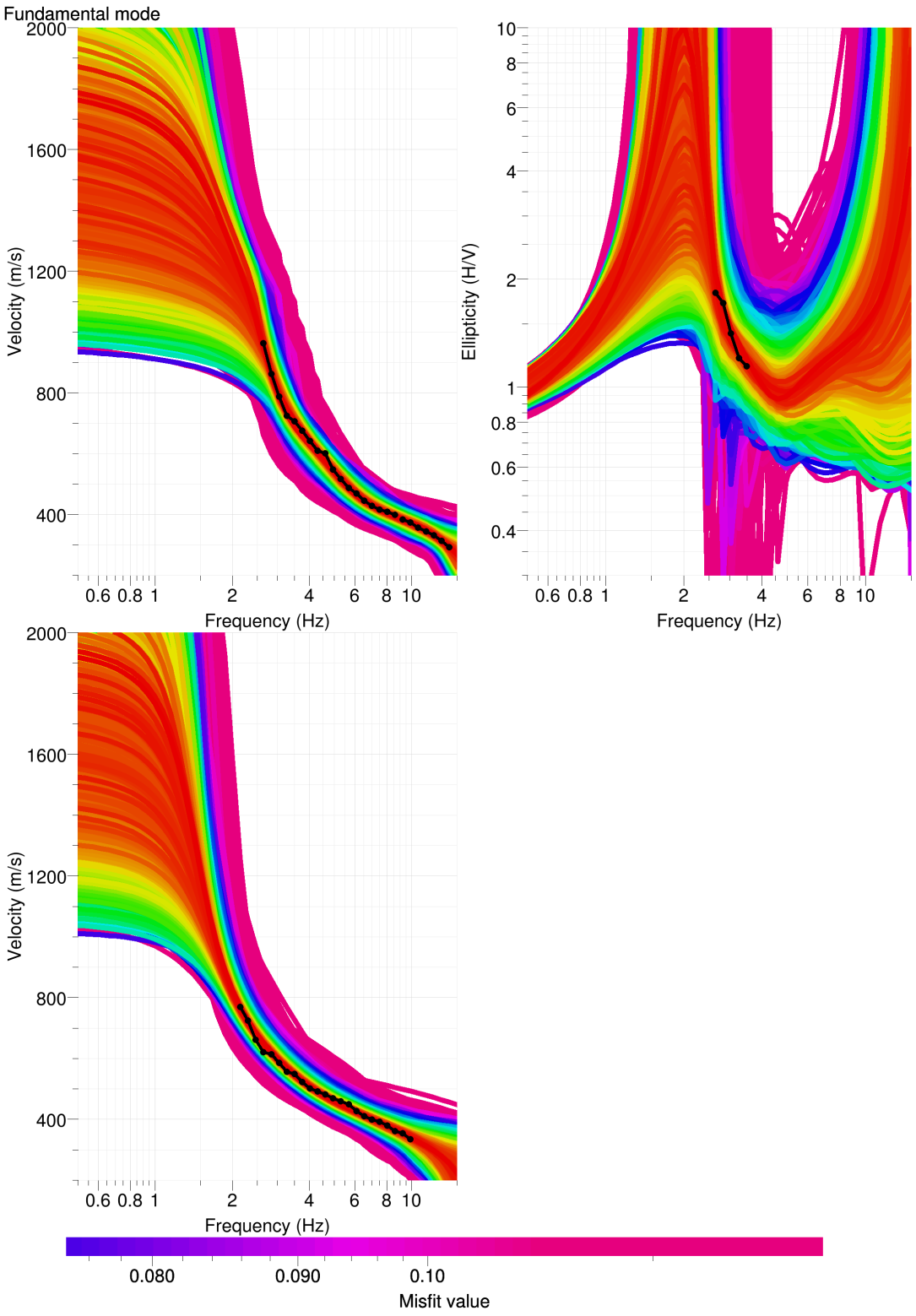

Figure 17: Comparison between inverted models and measured Rayleigh and Love modes and corresponding ellipticity, fixed layer depth strategy.

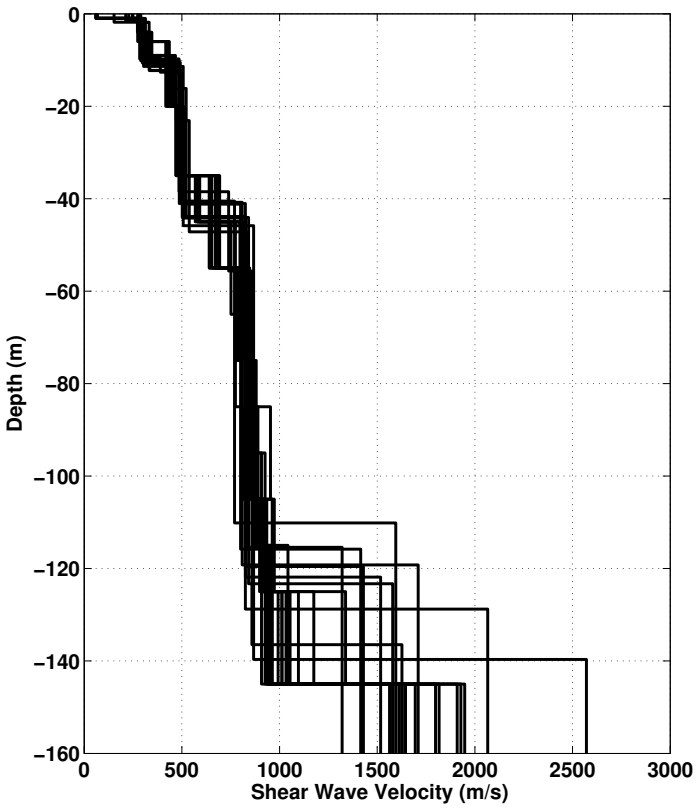

Figure 18: V_s ground profiles for the selected 25 best models.

7.2 Travel time average velocities and ground type

The distribution of the travel time average velocities at different depths was computed from the selected models. The uncertainty, computed as the standard deviation of the distribution of travel time average velocities for the considered models, is also provided, but its meaning is doubtful. $V_{s,30}$ is found to be $366\,\mathrm{m/s}$, which corresponds to class C in the Eurocode 8 [CEN, 2004] and SIA261 [SIA, 2003]. In theory, $V_{s,30}$ is exceeding the threshold for class C of EC8, but considering the uncertainties, engineering practice would consider it as C. For SIA261, this soil column also falls in the range of soil class E since $10\,\mathrm{m}$ of badly consolidated soil is sitting on top of sediments at $400 - 500\,\mathrm{m/s}$. However, it is doubtful that this class would be used in this case considering the low velocity contrast.

On the website of the Federal Office for Environment (Fig. 19), the indicated ground type is B. The complicated geology is taken into account on the map that is generally correct. In the deep Aare basin, with an upper part similar to the velocity profiles retrieved here, the ground type is C. Parts without the low velocity moraine cover are considered as B, which is debatable, since C would have been still correct ($V_s \approx 400 - 500\,\mathrm{m/s}$). More generally, this layer of fluvial sediments is systematically mapped as B. The moraine outcrops from the geology are categorized in A. For the rest of the map, if the bedrock depth was greater than $30\,\mathrm{m}$, it was considered as C, if not, is was categorized in E. The only exception is the area of the station SBERN, unexpectedly classified in B.

	Mean (m/s)	**Uncertainty (m/s)**
$V_{s,5}$	213	55
$V_{s,10}$	254	30
$V_{s,20}$	325	28
$V_{s,30}$	366	25
$V_{s,40}$	397	18
$V_{s,50}$	433	18
$V_{s,100}$	567	16
$V_{s,150}$	-	-
$V_{s,200}$	-	-

Table 7: Travel time averages at different depths from the inverted models. Uncertainty is given as one standard deviation from the selected profiles.

7.3 SH transfer function and quarter-wavelength velocity

The quarter-wavelength velocity approach [Joyner et al., 1981] provides, for a given frequency, the average velocity at a depth corresponding to 1/4 of the wavelength of interest. It is useful to identify the frequency limits of the experimental data (minimum frequency in dispersion curves at $2.1\,\mathrm{Hz}$ here). The results using this proxy show that the dispersion curves constrain the profiles down to $54\,\mathrm{m}$ (Fig. 20). Moreover, the quarter wavelength impedance-contrast introduced by Poggi et al. [2012a] is also displayed in the figure. It corresponds to the ratio between two quarter-wavelength average velocities, respectively from the top and the bottom

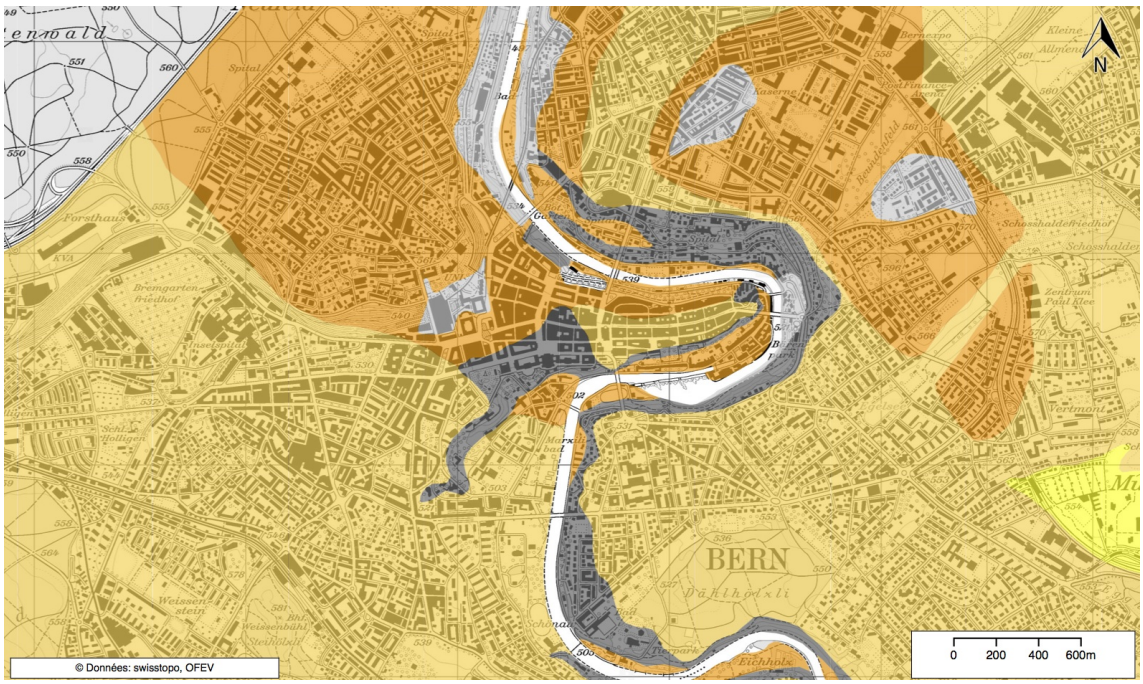

Figure 19: SIA261 ground types according to the Federal Office for Environment (yellow: D, light orange: C, orange: E, dark grey: B, light grey: A.

part of the velocity profile, at a given frequency [Poggi et al., 2012a]. It shows a trough (inverse shows a peak) at the resonance frequency (too low for this figure).
Moreover, the theoretical SH-wave transfer function for vertical propagation [Roesset, 1970] is computed from the inverted profiles. It is compared to the quarter-wavelength amplification [Joyner et al., 1981], that however cannot take resonances into account (Fig. 21). In this case, the models are predicting an amplification up to a factor of 4 at 1.6, 3.8 and 6.5 Hz, with respect to the lowest layer in the profile.

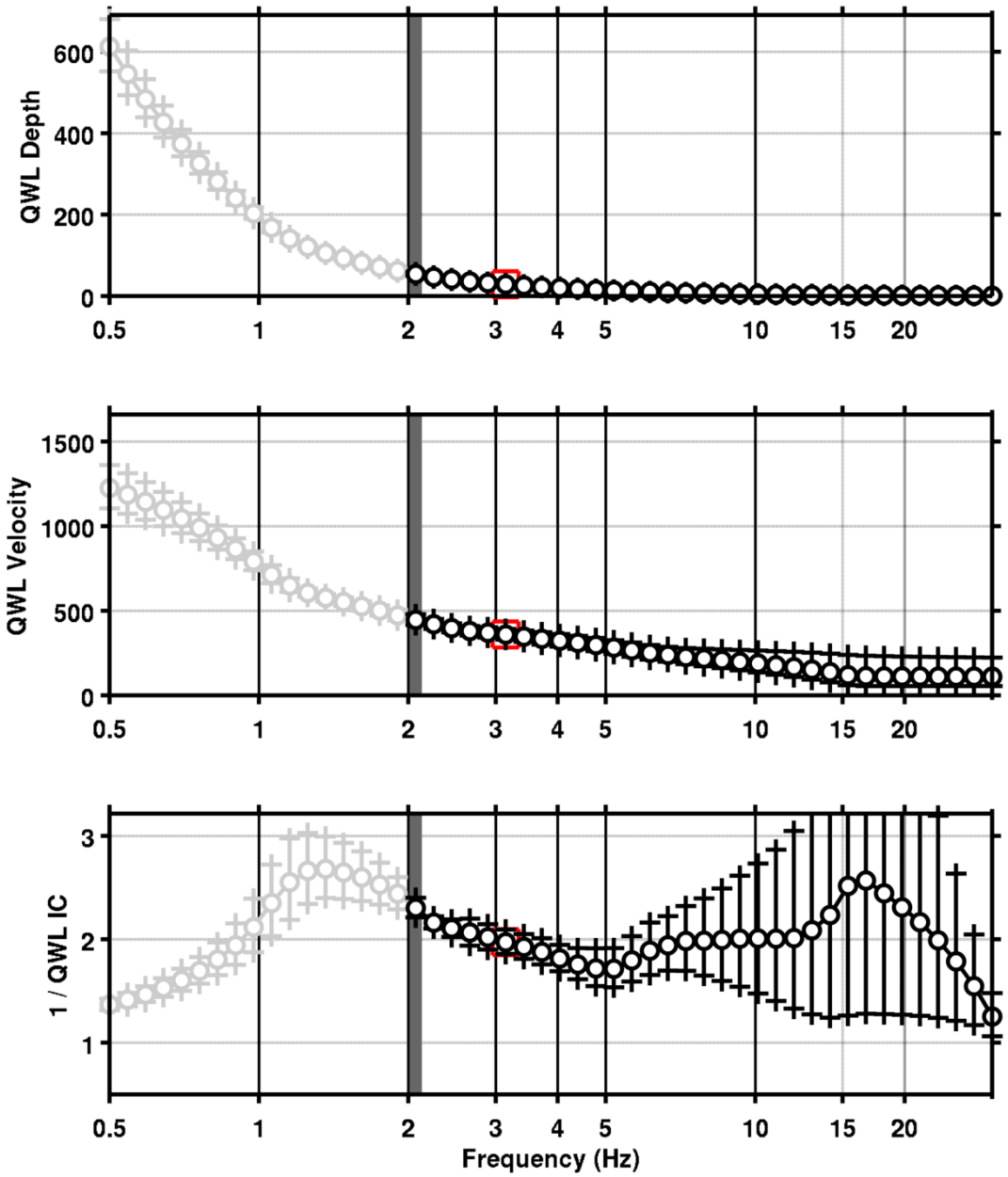

Figure 20: Quarter wavelength velocity representation of the velocity profile (top: depth, centre: velocity, bottom: inverse of the impedance contrast). Black curve is constrained by the dispersion curves, light grey is not constrained by the data. Red square is corresponding to $V_{s,30}$.

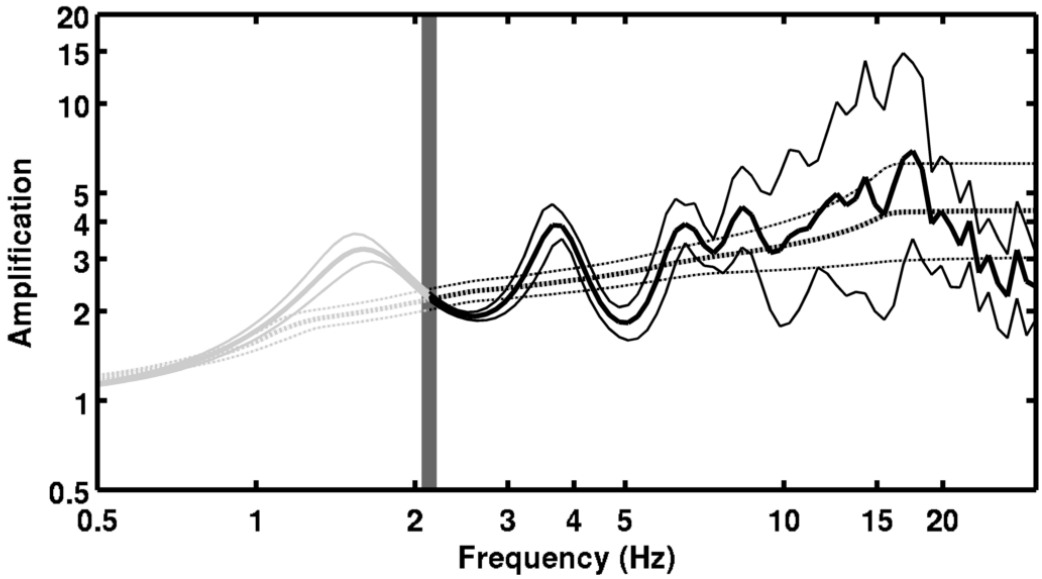

Figure 21: Theoretical SH transfer function (solid line) and quarter wavelength impedance contrast (dashed line) with their standard deviation. Significance of the greyshades is detailed in Fig. 20.

8 Conclusions

Geology and single station measurements were correlated in the city of Bern. The interface between the molasse rock and the Quaternary sediments is responsible for the major peak in the H/V spectra although a low-frequency peak at $0.8\,\mathrm{Hz}$ is also noticed and interpreted as an interface within the molasse rock at $300 - 400\,\mathrm{m}$ depth. A detailed mapping of the depth of the Quaternary sediments in Bern, extremely variable, would be necessary to estimate accurately the ground motion amplification in the city. SSMNet station SBERN, installed close to the Federal Palace is therefore representative only for a limited area.
The array measurements presented in this study were successful in deriving a velocity model for the site of the SBERN station. We found a first layer with low velocity around $270\,\mathrm{m/s}$ for the first 10 meters made of moraine, a second layer with velocity of $400 - 500\,\mathrm{m/s}$ corresponding to fluvial sediments and finally the molasse rock at $40\,\mathrm{m}$ depth. This interface corresponds to a resonance peak at $2\,\mathrm{Hz}$. The velocity of the molasse is $800\,\mathrm{m/s}$ down to $120\,\mathrm{m}$ and increases below. The lower frequency resonance ($0.8\,\mathrm{Hz}$) corresponding to the deeper layer at $300 - 400\,\mathrm{m}$ depth was observed as well but could not be constrained with these measurements.
$V_{s,30}$ is $366\,\mathrm{m/s}$, which would corresponds to ground type C in the Eurocode 8 [CEN, 2004] and SIA261 [SIA, 2003], even if it is debatable. The theoretical 1D SH transfer function and impedance contrast of the quarter-wavelength velocity computed from the inverted profiles show moderate amplifications at some resonance frequencies. Recordings on the new station will allow to compare to these simple models.

Acknowledgements

The authors thank Lea Kiefer who performed the single station measurement and help during the array measurements.

References

Sylvette Bonnefoy-Claudet, Fabrice Cotton, and Pierre-Yves Bard. The nature of noise wavefield and its applications for site effects studies. *Earth-Science Reviews*, 79(3-4): 205–227, December 2006. ISSN 00128252. doi: 10.1016/j.earscirev.2006.07.004. URL http://linkinghub.elsevier.com/retrieve/pii/S0012825206001012.

Jan Burjánek, Gabriela Gassner-Stamm, Valerio Poggi, Jeffrey R. Moore, and Donat Fäh. Ambient vibration analysis of an unstable mountain slope. *Geophysical Journal International*, 180(2):820–828, February 2010. ISSN 0956540X. doi: 10.1111/j.1365-246X.2009.04451.x. URL http://doi.wiley.com/10.1111/j.1365-246X.2009.04451.x.

J. Capon. High-Resolution Frequency-Wavenumber Spectrum Analysis. *Proceedings of the IEEE*, 57(8):1408–1418, 1969.

CEN. *Eurocode 8: Design of structures for earthquake resistance - Part 1: General rules, seismic actions and rules for buildings*. European Committee for Standardization, en 1998-1: edition, 2004.

Donat Fäh, Fortunat Kind, and Domenico Giardini. A theoretical investigation of average H / V ratios. *Geophysical Journal International*, 145:535–549, 2001.

Donat Fäh, Gabriela Stamm, and Hans-Balder Havenith. Analysis of three-component ambient vibration array measurements. *Geophysical Journal International*, 172(1):199–213, January 2008. ISSN 0956540X. doi: 10.1111/j.1365-246X.2007.03625.x. URL http://doi.wiley.com/10.1111/j.1365-246X.2007.03625.x.

Donat Fäh, Marc Wathelet, Miriam Kristekova, Hans-Balder Havenith, Brigitte Endrun, Gabriela Stamm, Valerio Poggi, Jan Burjanek, and Cécile Cornou. Using Ellipticity Information for Site Characterisation Using Ellipticity Information for Site Characterisation. Technical report, NERIES JRA4 Task B2, 2009.

William B. Joyner, Richard E. Warrick, and Thomas E. Fumal. The effect of Quaternary alluvium on strong ground motion in the Coyote Lake, California, earthquake of 1979. *Bulletin of the Seismological Society of America*, 71(4):1333–1349, 1981.

Katsuaki Konno and Tatsuo Ohmachi. Ground-Motion Characteristics Estimated from Spectral Ratio between Horizontal and Vertical Components of Microtremor. *Bulletin of the Seismological Society of America*, 88(1):228–241, 1998.

Valerio Poggi and Donat Fäh. Estimating Rayleigh wave particle motion from three-component array analysis of ambient vibrations. *Geophysical Journal International*, 180(1):251–267, January 2010. ISSN 0956540X. doi: 10.1111/j.1365-246X.2009.04402.x. URL http://doi.wiley.com/10.1111/j.1365-246X.2009.04402.x.

Valerio Poggi, Benjamin Edwards, and D. Fah. Characterizing the Vertical-to-Horizontal Ratio of Ground Motion at Soft-Sediment Sites. *Bulletin of the Seismological Society of America*, 102(6):2741–2756, December 2012a. ISSN 0037-1106. doi: 10.1785/0120120039. URL http://www.bssaonline.org/cgi/doi/10.1785/0120120039.

Valerio Poggi, Donat Fäh, Jan Burjanek, and Domenico Giardini. The use of Rayleigh-wave ellipticity for site-specific hazard assessment and microzonation: application to the city of Lucerne, Switzerland. *Geophysical Journal International*, 188(3):1154–1172, March 2012b. ISSN 0956540X. doi: 10.1111/j.1365-246X.2011.05305.x. URL `http://doi.wiley.com/10.1111/j.1365-246X.2011.05305.x`.

J.M. Roesset. Fundamentals of soil amplification. In R. J. Hansen, editor, *Seismic Design for Nuclear Power Plants*, pages 183–244. M.I.T. Press, Cambridge, Mass., 1970. ISBN 978-0-262-08041-5. URL `http://mitpress.mit.edu/catalog/item/default.asp?ttype=2\&tid=5998`.

SIA. *SIA 261 Actions sur les structures porteuses*. Société suisse des ingénieurs et des architectes, Zürich, sia 261:20 edition, 2003.

A. Sommaruga, U. Eichenberger, and F. Marillier. Seismic Atlas of the Swiss Molasse Basin. *Matériaux pour la Géologie de la Suisse*, 44, 2012.

Marc Wathelet. An improved neighborhood algorithm: Parameter conditions and dynamic scaling. *Geophysical Research Letters*, 35(9):1–5, May 2008. ISSN 0094-8276. doi: 10.1029/2008GL033256. URL `http://www.agu.org/pubs/crossref/2008/2008GL033256.shtml`.